Eur. Phys. J. Special Topics **226**, 1751–1764 (2017)

DOI: 10.1140/epjst/e2017-70055-y

THE EUROPEAN PHYSICAL JOURNAL SPECIAL TOPICS

Regular Article

# Generalized Lorenz equations on a three-sphere

Yoshitaka Saiki[1,2], Evelyn Sander[3,a], and James A. Yorke[4]

[1] Graduate School of Commerce and Management, Hitotsubashi University, Saiki, Japan
[2] JST, PRESTO, Sander and Yorke, USA
[3] Department of Mathematical Sciences, George Mason University, 22030 Fairfax, USA
[4] University of Maryland, College Park, Maryland 20742, USA

Received 13 February 2017 / Received in final form 27 March 2017
Published online 21 June 2017

**Abstract.** Edward Lorenz is best known for one specific three-dimensional differential equation, but he actually created a variety of related $N$-dimensional models. In this paper, we discuss a unifying principle for these models and put them into an overall mathematical framework. Because this family of models is so large, we are forced to choose. We sample the variety of dynamics seen in these models, by concentrating on a four-dimensional version of the Lorenz models for which there are three parameters and the norm of the solution vector is preserved. We can therefore restrict our focus to trajectories on the unit sphere $S^3$ in $\mathbb{R}^4$. Furthermore, we create a type of Poincaré return map. We choose the Poincaré surface to be the set where one of the variables is 0, i.e., the Poincaré surface is a two-sphere $S^2$ in $\mathbb{R}^3$. Examining different choices of our three parameters, we illustrate the wide variety of dynamical behaviors, including chaotic attractors, period doubling cascades, Standard-Map-like structures, and quasiperiodic trajectories. Note that neither Standard-Map-like structure nor quasiperiodicity has previously been reported for Lorenz models.

## 1 Three Lorenz systems

Edward Lorenz introduced polynomial systems of differential equations in a series of papers [1–7]. These equations all are dissipative, in the sense that all trajectories eventually end up in a finite size ball. The dynamics are chaotic for some parameter choices. While Lorenz justified these systems in terms of their being highly simplified meteorological or fluid-flow models, they are so severely simplified as to have little concrete practical use in meteorology. Regardless, in the intervening time, Lorenz equations have had a significant scientific impact, and their importance resides largely in their interesting dynamical behaviors. In this paper, we develop an overlying framework for the Lorenz systems which additionally produces a whole family of related differential equations. We call systems that fit into this framework generalized Lorenz

[a] e-mail: esander@gmu.edu

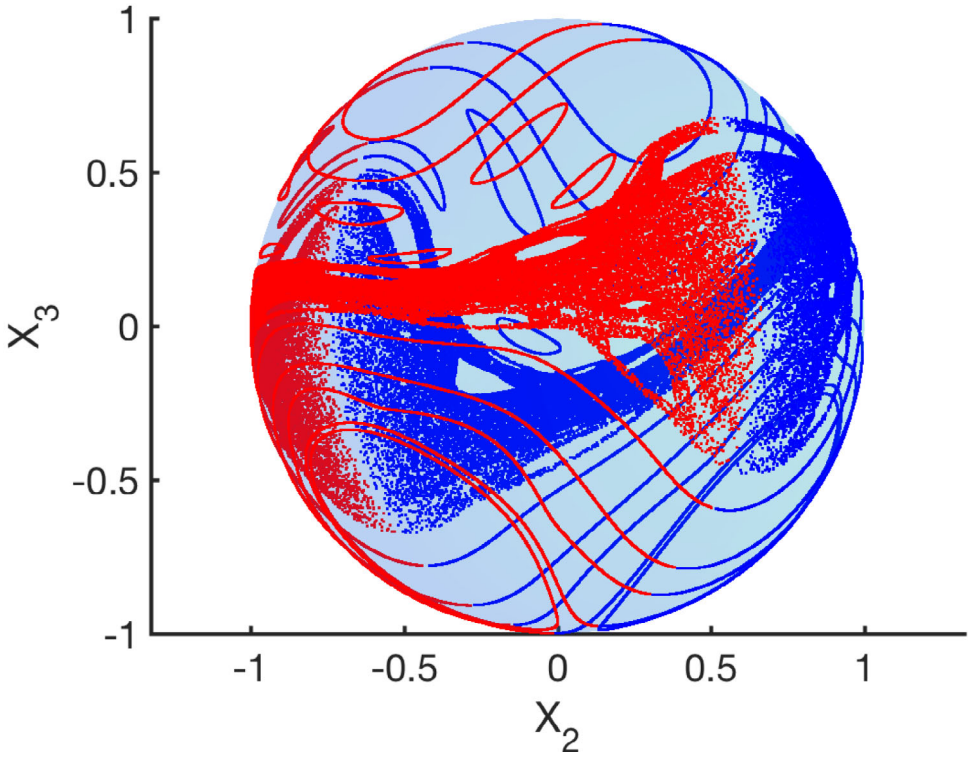


**Fig. 1.** Quasiperiodicity and chaos in the Poincaré Map on $S^2$ for GLE-4 with section $X_1 = 0$. Here we investigate trajectories of the 4-dimensional Generalized Lorenz Equation GLE-4, (given in Eq. (1) shown in this image for $\beta = 6$, $\rho = 8$, and $\gamma = 0$). We use initial conditions for which $\|\mathbf{X}\| = 1$. Since the norm $\|\mathbf{X}(t)\|$ remains constant, trajectories remain on the unit sphere, denoted $S^3$. To reduce the dimension by one, we only plot trajectories at those times when $X_1(t) = 0$, giving us a type of Poincaré map on the two-dimensional sphere $S^2$ shown here, given by $X_2^2 + X_3^2 + X_4^2 = 1$. We plot a Poincaré map point $(X_2, X_3)$ in a lighter color (red online) when the derivative $X_1'$ is positive and darker color (blue online) when negative. The colors are brighter (red and blue online) on the upper hemisphere $X_4 > 0$ and dull when $X_4 < 0$. Ten trajectories are shown here, nine of which are quasiperiodic. The full trajectory of each of the nine is a torus and here we show only the smooth curves where the torus intersects $X_1 = 0$. There is also one chaotic trajectory which can be seen wrapping around $S^2$ where $X_3 \approx 0$.

equations or Lorenz-like models. We start by developing the family of generalized Lorenz equations.

**A generalized Poincaré map.** The trajectories can be viewed using a Poincaré return map; see Figure 1. Using a Poincaré map reduces the dimension by 1, reducing the 3-sphere to a 2-sphere when we use the Poincaré surface such as $X_1 = 0$. Of course it is possible that even if a trajectory has its initial point on this surface, it may never return to the surface, such as might occur if there is an attractor that does not intersect the surface. In fact, an example of this phenomenon occurs for Poincaré's original return map, which was created for the circular restricted three-body problem. That surface of section only captures trajectories that cross the line between the two major bodies. The Lagrange Points L4 and L5 are equilibria that form equilateral

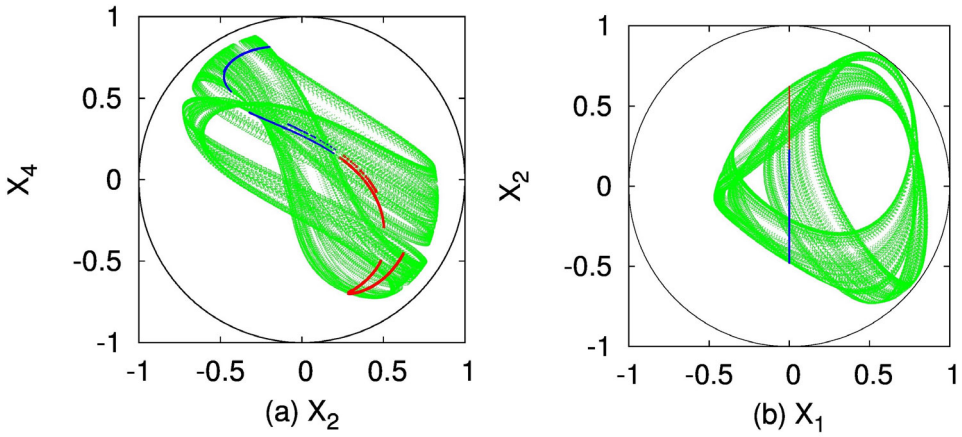


**Fig. 2.** Ribbon-like chaotic attractor in Lorenz $S^3$ Map. Both figures depict the same trajectory of the GLE-4 system (Eq. (1)) with norm 1 in light gray (green online) for $t > 0$, where $\beta = 1$, $\rho = 4.3$, and $\gamma = 1$. The Poincaré return map trajectory for the surface $X_1 = 0$ is also shown: the trajectory is plotted in a darker color (red or blue online) only when $X_1 = 0$, where red denotes points for which $X_1' > 0$ and blue $X_1' < 0$. Since we are unable to graph all four coordinates, we only show the projection of the trajectory to the $X_2X_4$-plane (a) and also to the $X_1X_2$-plane (b). This trajectory has a positive Lyapunov exponent and the light gray (green online) set is a chaotic attractor. Section 3 contains a bifurcation diagram containing this parameter value in the chaotic region. The attractor has Kaplan-Yorke dimension 2.11 on $S^3$.

triangles with the two massive bodies. All trajectories that stay close to L4 or L5 never cross the Poincaré surface.

We will then explore the variety of dynamical behaviors exhibited by members of this family, such as the chaos in Figure 2 and the quasiperiodicity in Figure 3, and use a Poincaré map to understand the dynamics better (see Fig. 1), with the caveat that the full family is so rich that we can only explore some examples. In particular, we restrict our numerics to the following system of equations, which we will derive in detail in Section 3. We refer to this system as GLE-4, the generalized Lorenz equations in dimension 4.

$$\begin{aligned} X_1' &= X_4X_2 - X_3X_4 + \beta(X_2 - X_4) + \gamma(X_2^2 - X_4X_1) \\ X_2' &= \rho X_1X_3 - X_4X_1 + \beta(X_3 - X_1) + \gamma(X_3^2 - X_1X_2) \\ X_3' &= X_2X_4 - \rho X_1X_2 + \beta(X_4 - X_2) + \gamma(X_4^2 - X_2X_3) \\ X_4' &= X_3X_1 - X_2X_3 + \beta(X_1 - X_3) + \gamma(X_1^2 - X_3X_4). \end{aligned} \tag{1}$$

**The general form.** For a dimension $N \geq 3$, let $\mathbf{X} = (X_1, \cdots, X_N)$, and let

$$Q(\mathbf{X}) = \frac{1}{2}\|\mathbf{X}\|^2 = \frac{1}{2}\sum_{i=1}^{N} X_i^2. \tag{2}$$

Lorenz designed a variety of equations such that $\frac{d}{dt}Q(\mathbf{X}(t)) < 0$ whenever $\|\mathbf{X}(t)\|$ is sufficiently large. In particular, Lorenz considered quadratic systems with the

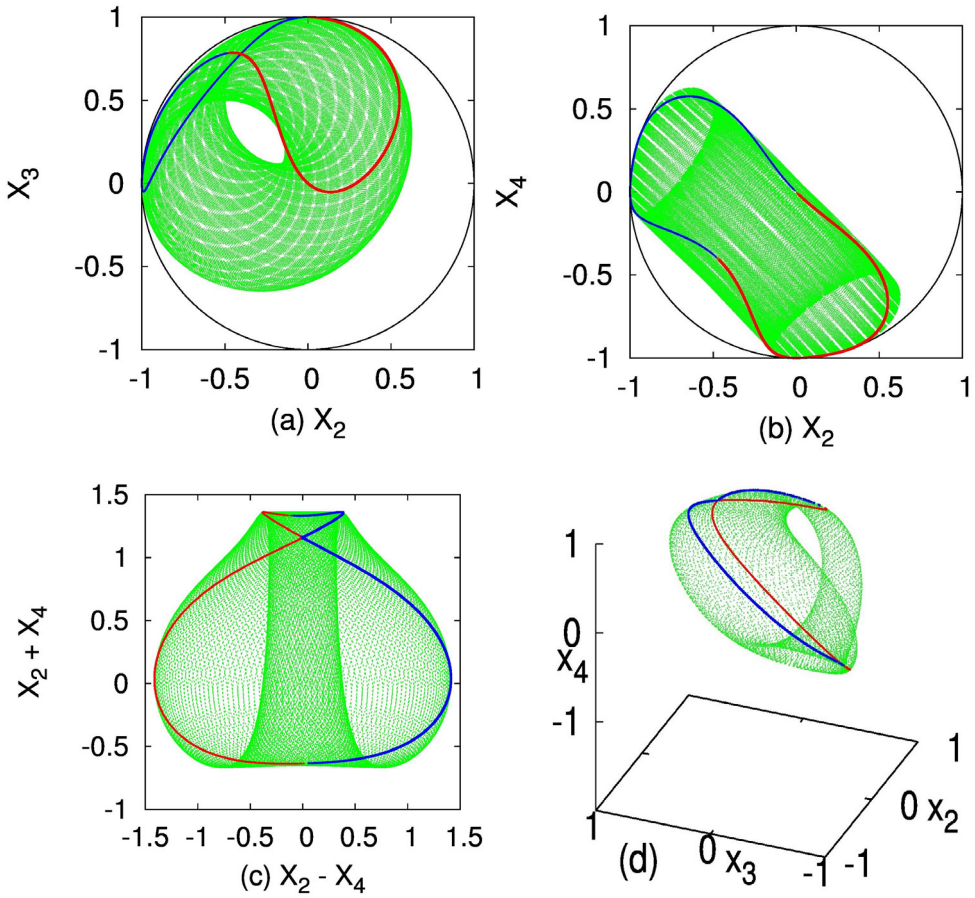


**Fig. 3.** Quasiperiodic flow in Lorenz $S^3$ Map. The images (a, b) depict different projections of a trajectory of the GLE-4 system (Eq. (1)) for $\beta = 6$, $\rho = 1$, and $\gamma = 0$. The trajectory, plotted in light gray (green online), has initial condition $X_1 = X_2 = X_4 = 0$ and $X_3 = 1$. The dark curve (blue and red online) shows the trajectory points where the trajectory intersects the Poincaré surface $X_1 = 0$. We plot such points in red when $X_1' > 0$ and blue when $X_1' < 0$. The images (c, d) show projections of another single trajectory with initial condition $X_1 = 0; X_2 = X_3 = X_4 = 1/\sqrt{3}$. For both initial conditions, the Poincaré map trajectories appear to densely fill "topological circles" (i.e., closed curves without self intersections) in $S^2$ (though these curves can appear to self-intersect), indicating that these are quasiperiodic trajectories rather than chaotic ones. In fact all Lyapunov exponents (for vectors tangent to the surface) for both trajectories are 0 (to within expected numerical accuracy).

general form[1]

$$\frac{dX_i}{dt} = X_i' = f_i(\mathbf{X}), \text{ where}$$

$$f_i(\mathbf{X}) = \sum_{j=1}^{N}\sum_{k=1}^{N} a_{i,j,k} X_j X_k - \sum_{j=1}^{N} b_{i,j} X_j + c_i, \tag{3}$$

[1] or a minor variation of it in 1963.

for $i, j, k = 1, \cdots, N$. The indexed lower case letters $a, b$, and $c$ in our equations indicate constants.

Notice that

$$Q'(\mathbf{X}) := \frac{d}{dt}Q(\mathbf{X}(t)) = \sum_{j=1}^{N} X_j X_j' = \sum_{j=1}^{N} X_j f_j(\mathbf{X}).$$

**Lorenz 1963.** The first equation of this type in which Lorenz reported chaotic behavior was [1]

$$\begin{aligned} X' &= -\sigma X + \sigma Y \\ Y' &= -XZ + rX - Y \\ Z' &= +XY - bZ \end{aligned} \tag{4}$$

where the variant of $Q$ that Lorenz used is $\hat{Q} = \frac{1}{2}[X^2 + Y^2 + (Z - \sigma - r)^2]$ and with $\sigma, b, r > 0$. Hence

$$\hat{Q}' = -\sigma X^2 - Y^2 - bZ^2 + \sigma bZ + brZ.$$

In $\hat{Q}$ from equation (4), the term $-XZ$ in the $Y'$ equation, and the $+XY$ term in the $Z'$ equation (the magenta terms in the online color version) yield cubic terms $\pm XYZ$ which cancel each other (total to 0) plus some quadratic terms. In summary the terms $-\sigma X^2 - Y^2 - bZ^2$ (in blue online) in $\hat{Q}'$ are quadratic and negative definite while the terms $+\sigma bZ + brZ$ (in red online) are linear in $Z$. Hence far from the origin the negative quadratic terms dominate so that $\hat{Q}' < 0$. As a result trajectories remain bounded (inside a ball of radius $|\sigma + r|$), and there has to be an attractor. Lorenz used the same ideas in 1984 and 1996.

This equation has been widely referenced as a prototype for chaotic behavior [8–11]. See for example an application to partial control [13].

In the rest of this paper we restrict attention to the simpler case where $Q$ is given by equation (2). As noted in Lorenz's 1963 paper (see his Eq. (28)), we can change variables above changing $\hat{Q}$ into $Q$ by letting $\hat{Z} = Z - \sigma - r$ so that $Q(X, Y, \hat{Z})$ is a sum of squares. For this choice of $Q$, the $\sigma$ and $r$ terms vanish in $Q'$.

**Lorenz 1984.** In a later paper [4], Lorenz used the equation

$$\begin{aligned} X' &= -Y^2 - Z^2 - aX + c \\ Y' &= +XY - bXZ - Y + d \\ Z' &= +bXY + XZ - Z \end{aligned} \tag{5}$$

with constants $a, b, c, d$ where $a > 0$. Note that to preserve most of Lorenz's notation, we are abusing terminology here so that now $X$ is a scalar. When computing $\hat{Q}'$ from equation (5), the pair consisting of $-Y^2$ in the $X'$ equation and $+XY$ in the $Y'$ equation (red terms online) yield $\pm XY^2$ and cancel. Similarly, the two terms $-Z^2$ in the $X'$ equation and $+XZ$ in the $Z'$ equation (blue terms online) yield $\pm XZ^2$ and cancel. Finally, the terms $-bXZ$ in the $Y'$ equation and $+bXY$ in the $Z'$ equation (cyan terms online) yield $\pm bXYZ$ and cancel. Hence $Q' = -(aX^2 + Y^2 + Z^2) + cX + dY$. Again the quadratic terms of $Q'$ dominate the linear ones $cX + dY$ for points sufficiently far from the origin, so there is again an attractor.

**Lorenz 1996 = Lorenz 1998.** Lorenz in 1996 [6] and Lorenz-Emanuel in 1998 [7] proposed an $N$-dimensional system of equations with symmetry mod$N$. It is the following very simplified weather model

$$X_j' = X_{j-1}X_{j+1} - X_{j-2}X_{j-1} - bX_j + c(\text{subscripts mod } N) \tag{6}$$

that has $N$ variables and are invariant under the rotation $j \mapsto j+1 \bmod N$; that is $X_j = X_{j+N} = X_{j-N}$. We sometimes write "subscripts mod $N$" to represent this convention. This system has been used to explore the nature of high dimensional attractors, where the dimension can be computed numerically using the Kaplan-Yorke formula.[2]

In the first of these papers [6], Lorenz stated "the variables may be thought of as values of some atmospheric quantity in $N$ sectors of a latitude circle. The physics of the atmosphere is present only to the extent that there are external forcing and internal dissipation, simulated by the constant and linear terms, while the quadratic terms, simulating advection, together conserve the total energy" (which we call $Q$). "We assume that $N > 3$; the equations are of little interest otherwise. The variables have been scaled to reduce the coefficients in the quadratic and linear terms to unity ...."

Lorenz makes use of the fact that $Q'$ derived from equation (6) includes the sum

$$\sum_j [X_{j-1}X_jX_{j+1} - X_{j-2}X_{j-1}X_j],$$

which is a telescoping sum, and since we have assumed that $X_{N-1}X_NX_{N+1} = X_{-1}X_0X_1$, the sum is equal to 0.

## 2 Generalized Lorenz equations

There is clearly a theme in the nature of the terms in the above equations, so we now explore generalizations. We can generalize equation (6) to

$$\begin{aligned} X'_j = &\sum_{i,k=1}^{N} a_{i,k}[X_{j+i}X_{j+k} - X_{j+i-k}X_{j-k}] \\ &+ \sum_{k=1}^{N} \beta_k[X_{j+k} - X_{j-k}] - bX_j + c \text{ (subscripts mod } N). \end{aligned} \tag{7}$$

When we set $i = -1$, $k = 1$ and $a_{-1,1} = 1$ in this equation, the terms $X_{j-1}X_{j+1} - X_{j-2}X_{j-1}$ (terms in red online) become in equation (6) the $a_{i,k}$ terms (terms in red online).

The $a_{i,k}$ (red online) terms cancel out in computing $Q'$ as do the $\beta_k$ (blue online) terms. By setting $i = 0$ in the $a_{i,k}$ (red) terms above, we obtain terms like the $-Z^2$ and $+XZ$ (blue) terms in equation (5) and obtain the terms

$$\sum_{k=1}^{N} a_{0,k}[X_jX_{j+k} - X_{j-k}^2] \text{ (subscripts mod } N).$$

**Pairs of terms that cancel in $Q'$.** We can choose the coefficients in equation (7) so that pairs cancel in $Q'$, as in the following pair of equations. Together they contribute 0 to $Q'$ for any function $g(\mathbf{X})$ (which is a constant in the Lorenz models)

$$\begin{aligned} X'_i &= X_j^2 g(\mathbf{X}) \\ X'_j &= -X_iX_j g(\mathbf{X}) \end{aligned} \tag{8}$$

[2] See [7], left column of page 403. See also related work on unstable dimension variability and shadowing for equation (6) in [12].

Then $X_iX_i' + X_jX_j' = 0$. Lorenz also adds globally dissipative terms to $X_i'$ of the form $-a_iX_i + \cdots$ where $a_i > 0$ so that $Q'$ has terms $\sum_j -a_jX_j^2$.

Pairs of terms for $i \neq j$ that contribute 0 to $Q'$ include

$$\begin{aligned} X_i' &= X_j \\ X_j' &= -X_i. \end{aligned} \tag{9}$$

Of course a constant multiplier $\alpha_{i,j}$ can be included for each pair of $i$ and $j$. Similarly:

$$\begin{aligned} X_i' &= X_jX_k \\ X_j' &= -X_iX_k \end{aligned} \tag{10}$$

where we may allow $k = i$ or $k = j$ but $i \neq j$. For example, for $j = k \neq i$, we pair square terms $X_j^2$ with quadratic products $-X_iX_j$ where $i \neq j$. In addition, for a 4-dimensional system, each equation $X_i'$ can have 3 terms of the form $X_j^2$, so there are 12 possible pairs of terms of the form

$$\begin{aligned} X_i' &= X_j^2 \\ X_j' &= -X_iX_j. \end{aligned} \tag{11}$$

**An axis of rotation for the quadratic terms.** For a more abstract approach see [14] and references to that paper. They show that if

(i) $F(\mathbf{X}) = (f_1, \cdots, f_N)$ in equation (3) is purely quadratic, i.e., where the coefficients $b_{i,j}$ and $c_i$ are 0; and
(ii) all solutions of the equation $\mathbf{X}' = F(\mathbf{X})$ are bounded,

then there must be some "axis vector" $\mathbf{X}_0 \neq 0$ for which $F(\mathbf{X}_0) = 0$. And of course then $F(\mathbf{X}) = 0$ for all $\mathbf{X}$ on the line containing $\mathbf{X}_0$ and the origin. This can be thought of as an axis of rotation, about which the solutions oscillate.

Whenever $\mathbf{X}_0 \neq 0$ and $F(\mathbf{X}_0) = \lambda\mathbf{X}_0$ for some $\lambda$, (ii) above implies $\lambda$ must be 0.

Using only the quadratic terms in the three Lorenz equations above, we can observe that in both the equations. (4), (5) of 1963 and 1984, $\mathbf{X}_0 = (1, 0, 0)$ is such an axis vector, while for equation (5) of 1996, $\mathbf{X}_0 = (1, \cdots, 1)$. In general axis vectors can be found using numerical methods of degree theory; see [15].

## 3 Our equation GLE-4 on $S^3$

In this section, we consider a subclass of generalized Lorenz equations such that trajectories are of constant norm. That is, we only choose terms such that $Q' \equiv 0$, so $\|\mathbf{X}\|$ is constant. Note that since each trajectory is restricted to a sphere of constant norm $\|\mathbf{X}\| = c$, in order to make chaos possible requires dimension $\geq 4$. In our 4-dimensional generalized Lorenz equation (which we call GLE-4) below, we restrict to dimension 4, and we consider trajectories such that for the initial condition, and thus the entire trajectory, $Q = \|\mathbf{X}\|^2/2 = 1/2$, meaning that the dynamics lie on a unit sphere $S^3$. We can have equations there like

$$\begin{aligned} X_j' =& [X_{j-1}X_{j+1} - X_{j-1}X_{j-2}] + \beta[X_{j+1} - X_{j-1}] \\ &+ \gamma[X_{j+1}^2 - X_{j-1}X_j] \text{ (subscripts mod } N). \end{aligned} \tag{12}$$

In $Q'$ the following terms occur twice, once positive and once negative, and the sum of these totals to zero:

$$\sum_{j=1}^{N} X_j X_{j-1} X_{j-2} + \beta X_j X_{j+1} + \gamma X_j X_{j+1}^2 \text{ (subscripts mod } N).$$

This follows from the fact that we are assuming the subscripts mod $N$ are equal. For example, $X_{N-1}X_N X_{N+1} = X_{-1}X_0X_1$, $X_N X_{N+1} = X_0X_1$, and $X_N X_{N+1}^2 = X_0X_1^2$. Thus all the terms of the telescoping sum cancel.

We now concentrate on the following 4-dimensional generalized Lorenz system such that all trajectories have constant norm. We focus on solutions on the invariant subset $S^3$ of $\mathbb{R}^4$. This leads to our main system of equations, GLE-4 which was given in the introduction. We repeat it here to avoid the reader needing to flip pages back and forth.

$$\begin{aligned} X_1' &= X_4X_2 - X_3X_4 + \beta(X_2 - X_4) + \gamma(X_2^2 - X_4X_1) \\ X_2' &= \rho X_1X_3 - X_4X_1 + \beta(X_3 - X_1) + \gamma(X_3^2 - X_1X_2) \\ X_3' &= X_2X_4 - \rho X_1X_2 + \beta(X_4 - X_2) + \gamma(X_4^2 - X_2X_3) \\ X_4' &= X_3X_1 - X_2X_3 + \beta(X_1 - X_3) + \gamma(X_1^2 - X_3X_4). \end{aligned} \tag{13}$$

While we have included constants $\beta$, $\gamma$, and $\rho$, clearly many more could be introduced. However, three constants are enough to experiment with, and this matches the number of constants in Lorenz's original equation (Eq. (4)). If $\beta = 0$, all terms are quadratic, so if $\mathbf{X}(t) = (X_1, X_2, X_3, X_4)(t)$ is a solution, then so is $\omega\mathbf{X}(\omega t)$. If instead $\rho = 1$, there is coefficient symmetry so the system can be written in the form of equation (1).

**Poincaré Return Maps for GLE-4.** Henri Poincaré introduced Poincaré return maps for the restricted three-body problem in order to reduce the dimension of the system. Instead of a flow on a generalized energy surface in $\mathbb{R}^4$, he defined a map in $\mathbb{R}^2$ by plotting trajectories as they crossed some surface such as $X_j = 0$, plotting only when the trajectory was passing through with a specified orientation, say $X_j' > 0$. Such a point determined a flow point in $\mathbb{R}^4$: because his energy surface was quadratic, there were two possibilities for $X_j'$ for a specified energy levels, one positive and one negative, and he chose the one with $X_j' > 0$. We consider here a Poincaré return map. However, unlike Poincaré we record all crossings of the Poincaré surface, as we will explain later is necessary.

The GLE-4 trajectories tend to be highly oscillatory, most often with each variable $X_j$ oscillating around 0. Hence for any $j$ we can plot the trajectory when $X_j = 0$ provided $X_j' > 0$ or better yet we can always plot the trajectory point when $X_j = 0$ and color code it according to the sign of $X_j'$. The surface where $X_j = 0$ is an "equator" of $S^3$, which is $S^2$, the two-dimensional sphere. Its projection onto the plane is a double covering of the unit disk. If we choose $j = 1$, we plot $(X_2, X_3)$ and we can recover $X_4 = \pm\sqrt{1 - (X_2^2 + X_3^2)}$ from the plotted point $(X_2, X_3)$ by choosing a plus sign when the plotted point is bright and minus when it is dull.

In summary, since our figures project the 2-sphere onto a disk, information is potentially lost as to which hemisphere the point is on, and that information must be retained if we are to reproduce the trajectory.

As with Figure 1, we sometimes plot Poincaré map points $(X_2, X_3)$ in two colors, say red when $X_1' > 0$ and blue when $X_1' < 0$. The map will be discontinuous in places where the vector field is tangent to the Poincaré surface, i.e., $X_1' = 0$. The boundary points between red and blue are such points of tangency.

**Table 1.** Table of parameters in Figures.

| Figure | $\beta$ | $\rho$ | $\gamma$ |
|---|---|---|---|
| 1 | 6 | 8 | 0 |
| 2 | 1 | 4.3 | 1 |
| 3 | 6 | 1 | 0 |
| 4 | 6 | 2, 2, 8, 10 | 0 |
| 5 | 6 | 2 | 0 |
| 6 | 1 | 4.5, 17 | 1 |
| 7 | 1,2,3,4 | 4.5 | 0 |
| 8 | 0 | 3.6, 1.0 | −0.3, 0.5 |
| 9 | 1 | (2, 18) | 1 |

**Dynamics of GLE-4.** We have made a variety of numerical experiments for various parameter combinations, and the resulting figures are summarized in Table 1. For example Figure 1, shows GLE-4 trajectories of a Poincaré return map where $\beta = 6$, $\rho = 8$, and $\gamma = 0$. The Poincaré surface is again given by $X_1 = 0$. The two different colors show the two different signs of $X_1'$. Here we show 15 distinct trajectories on the same graph. Some trajectories are topological circles (closed curves without self-intersections). They are quasiperiodic. However, there is also a trajectory which appears to fill a region densely and is chaotic (and it has a positive Lyapunov exponent).

Figure 2 depicts the trajectory of GLE-4 for continuous time $t$ starting at one initial condition for $\rho = 4.3$ and $\beta = \gamma = 1$. The Poincaré return map $X_1 = 0$ is also shown, where red denotes $X_1' > 0$ and blue denotes $X_1' < 0$. Since we are unable to graph all four coordinates simultaneously, we only show the projection of the same trajectory to the $X_2X_4$-plane and also to the $X_1X_2$-plane. The irregular chaotic structure of its Poincaré map trajectory gives a strong indication that this trajectory is chaotic. In fact we have computed its Lyapunov exponents and the attractor has Kaplan-Yorke dimension 2.11 when the equation is restricted to the three-sphere $S^3$. (That is, we are ignoring a zero Lyapunov exponent transverse to $S^3$.)

In this and subsequent figures, we show the Poincaré return map trajectories for the surface defined by $X_1 = 0$. We make the non-standard choice of showing for the trajectories hitting in both directions $X_1' > 0$ and $X_1' < 0$. For Poincaré the two directions consist of two widely separated pieces. However, in our case, the two directions are often mixed together in a connected set. This means that there is a curve of tangency points of the trajectory to the subspace $X_1 = 0$, i.e., $X_1' = 0$, meaning that our mapping is almost always discontinuous at these points of tangency as mentioned above.

Figure 3 depicts the trajectory of GLE-4 for $\rho = 1$, $\beta = 6$, $\gamma = 0$ starting at two different initial conditions (in different subfigures), where the Poincaré return map $X_1 = 0$ is depicted using the same color scheme as in Figure 2. For two different sets of initial conditions, we project the same four-dimensional trajectory in two different ways so as to compare the different views. In contrast to the previous figure, the trajectory densely fills a smooth curve, indicating that this is a quasiperiodic trajectory and not a chaotic trajectory.

Figures 4 and 5 show GLE-4 for $\beta = 6$, $\gamma = 0$. As in Figure 1 above, we only show the Poincaré return map projected to the $X_2X_3$-plane, again for the surface $X_1 = 0$. Note that since $\mathbf{X}$ is on the unit sphere $S^3$ in $\mathbb{R}^4$, and the Poincaré map has the condition $X_1 = 0$, we have that $X_2^2 + X_3^2 + X_4^2 = 1$, meaning that $(X_2, X_3, X_4)$ is on the sphere $S^2$ in $\mathbb{R}^3$. In this and other figures, we show the sphere $S^2$ so as to depict the location of the trajectories. In Figure 4, $\rho = 2, 8, 10$. As $\rho$ increases, the dynamics moves from purely quasiperiodic for $\rho = 2$ to a case of coexisting quasiperiodicity and

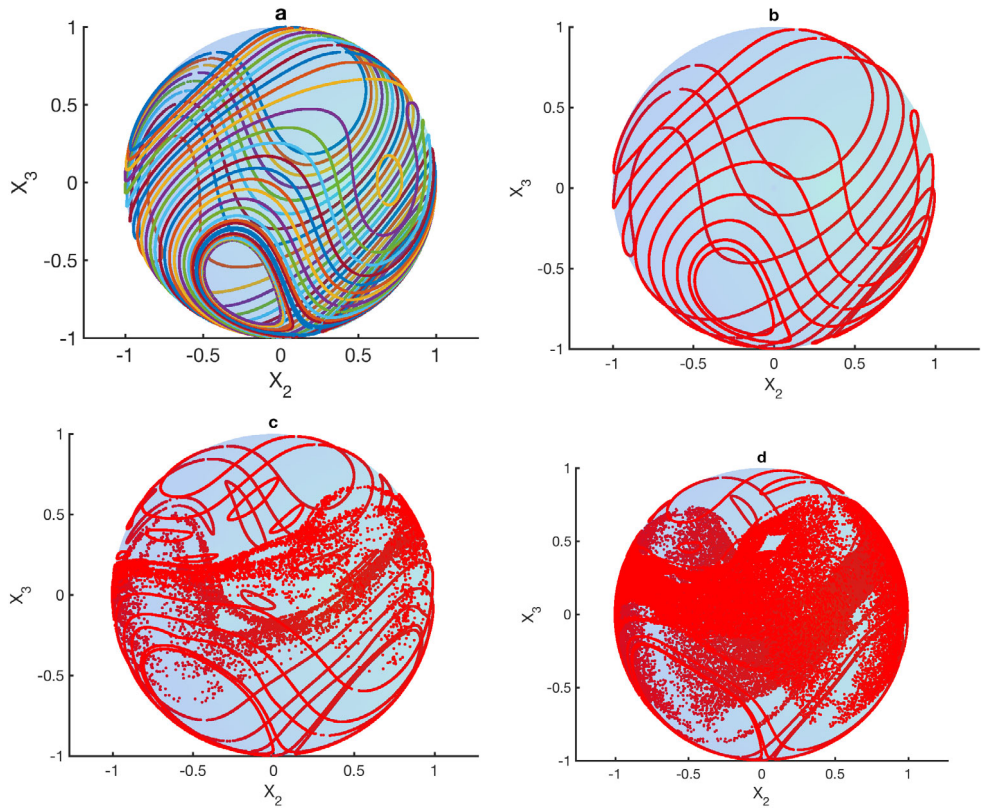


**Fig. 4.** Standard-Map-like dynamics for GLE-4. For the system GLE-4 (Eq. (1)), trajectories in the unit sphere $S^3$ in $\mathbb{R}^4$, we invoke the Poincaré return map for the Poincaré surface defined by $X_1 = 0$, which is a two-dimensional sphere $S^2$. The sphere is projected to the $X_2X_3$-plane. Image (a) uses different colors to show 30 distinct quasiperiodic orbits for $\beta = 6, \rho = 2, \gamma = 0$. In the rest of the figures, we graph ten distinct orbits, all in the same color. In all four figures, $\beta = 6$ and $\gamma = 0$, with $\rho = 2$, 8, 10 in (b,c,d) respectively. (Note that the parameters values are the same in (a) and (b).) We refer to the behavior seen here, in which there are coexisting quasiperiodic and chaotic orbits, as "Standard-Map-like".

chaotic behavior for $\rho = 8, 10$. We refer to this coexistence as **Standard-Map-like**, as it is reminiscent of the coexistence of quasiperiodicity and chaos as seen in the Standard Map, a well known map on the torus.

Figure 6 depicts orbits for GLE-4 for $\beta = 1$, $\rho = 4.5$, 17, and $\gamma = 1$. (See Fig. 9 for the bifurcation diagram for the corresponding parameter region.) In the $\rho = 4.5$ case, we see a ribbon-like chaotic attractor. For $\rho = 17$, the chaotic attractor still exhibits Cantor-set like bands, but it is unusually rich in structure.

Figure 7 shows GLE-4 trajectories for $\beta = 1, 2, 3, 4$, $\gamma = 0$, $\rho = 4.5$. For $\beta = 1$, there appears to be a dense trajectory. As $\beta$ grows, the asymptotic behavior becomes more localized, and for the last three $\beta$ values, we see Standard-Map-like coexistence of chaos and quasiperiodicity.

Figure 8 depicts trajectories for the purely quadratic GLE-4 system, namely when $\beta = 0$, which may be of special interest to some readers. In this case, we have found cases with chaos with complex phase portaits, as shown in.

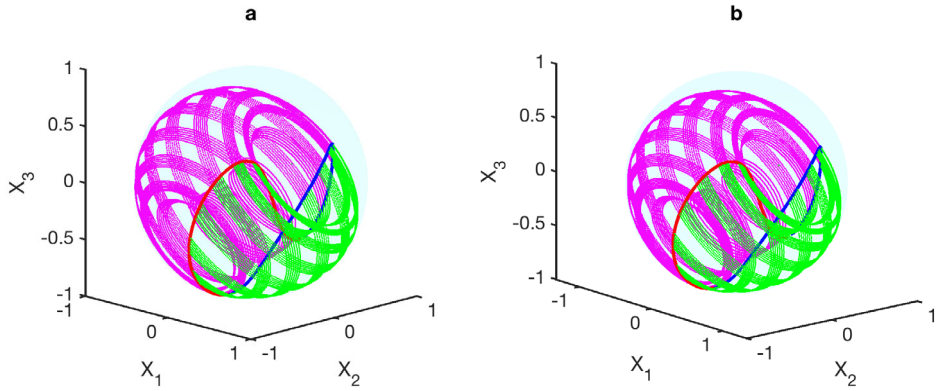


**Fig. 5.** A stereographic view of a quasiperiodic trajectory. For the same values as in Figures 4a and 4b, we show a trajectory of the system GLE-4 (Eq. (1)) in the three dimensional space $X_2X_3X_4$-space. The Poincaré return map points where $X_1 = 0$ are depicted as a dark curve (in blue online). The trajectory for $X_1 > 0$ is shown in light gray (green online), and $X_1 < 0$ in a darker color (magenta online). We have displayed two slightly different views of this torus projected to a three-dimensional space so that the reader can view it from two slightly different vantage points in order to better understand the complexity of the torus structure. The piece shown of the trajectory is short, leaving gaps in the torus that would fill in with more iterates.

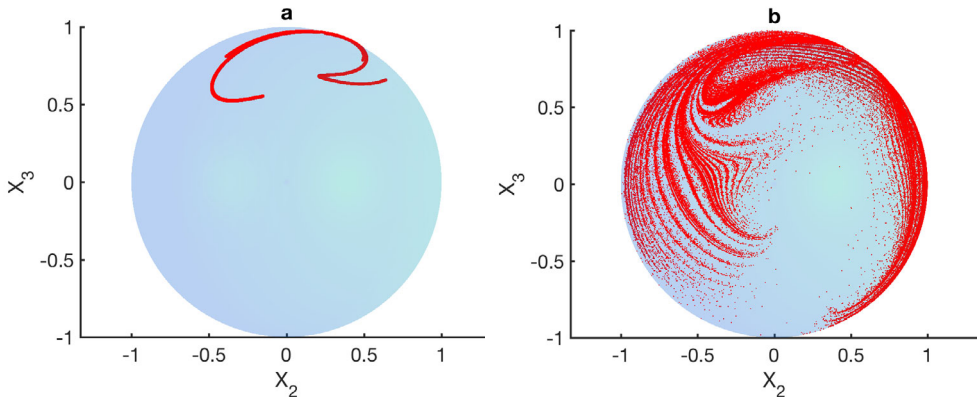


**Fig. 6.** Different varieties of chaotic attractors for GLE-4. This figure depicts the Poincaré return map $X_1 = 0$ for the GLE-4 system (Eq. (1)). The plot is a projection of the trajectory to the $X_2X_3$-plane. There is a Hénon-like chaotic attractor for $\beta = 1$, $\rho = 4.5$, $\gamma = 1$ (a), and a rather odd chaotic attractor at $\beta = 1, \rho = 17, \gamma = 1$ (b).

In Figure 9 we show a bifurcation diagram of the Poincaré return map of GLE-4 for $\beta = \gamma = 1$ and varying $\rho$. In particular, we plot $X_2$ along the vertical axis and $\rho$ along the horizontal axis. In the color version online, in blue, we show the return map for $X_1' > 0$, and in red, we plot the return map with $X_1' < 0$. Thus for example from $\rho = 2$ until approximately $\rho = 3$, there is a periodic orbit containing only one red and one blue point of the the Poincaré map. It is clear from this diagram that a period-doubling cascade occurs en route to chaos for $\rho$ between 2 and 4.3.

**Summary.** To summarize our findings, in this paper we have developed a general framework encompassing and extending a series of dissipative differential equation

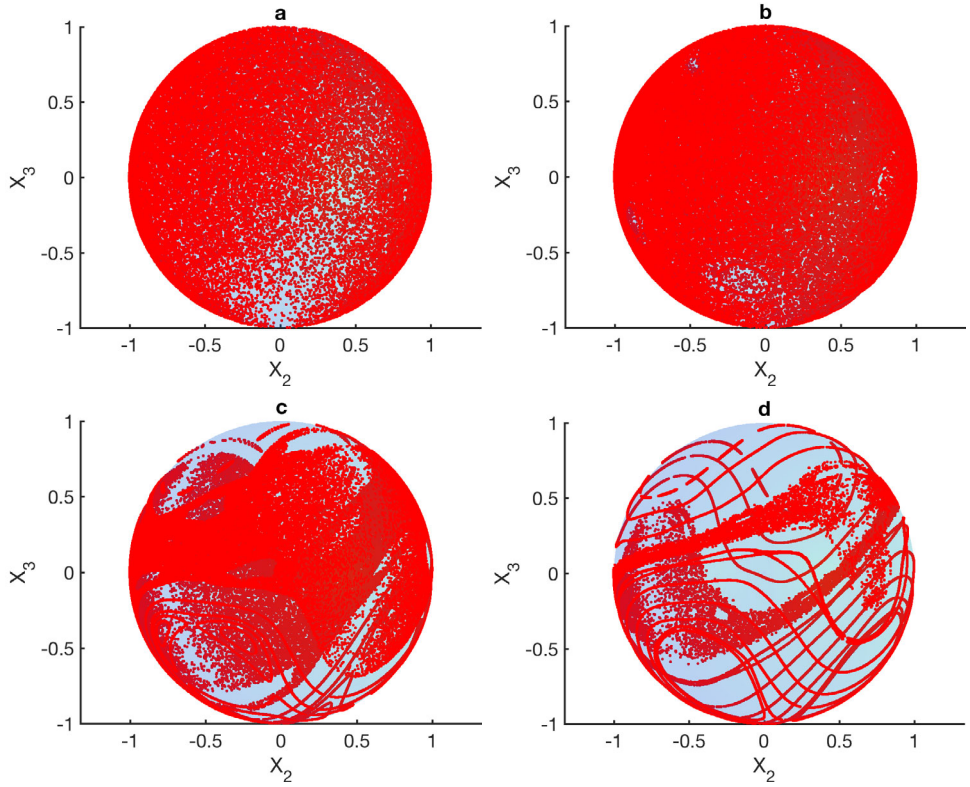


**Fig. 7.** Transition from dense chaotic orbits to Standard-Map-like behavior. Poincaré return map of trajectories for the GLE-4 system (Eq. (1)) for parameters $\beta = 1, 2, 3, 4$ in (a), (b), (c), (d) resp., and $\rho = 4.5$, $\gamma = 0$. All plots are projected to the $X_2X_3$-plane. We see a change from what appears to be a chaotic orbit that appears to be dense on the entire sphere – through progression of Standard-Map-like behavior that combines regions of chaos and quasiperiodicity.

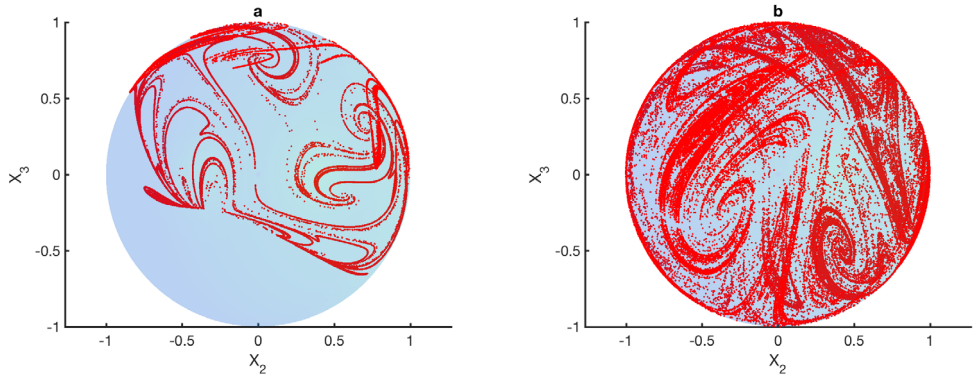


**Fig. 8.** The purely quadratic case for GLE-4. This figure depicts the Poincaré return map $X_1 = 0$ for the GLE-4 system (Eq. (1)). The plot is a projection of the trajectory to the $X_2X_3$-plane. Two chaotic attractors for $\beta = 0$: in (a) $\rho = 3.6$, $\gamma = -0.3$, and in (b) $\rho = 1.0$, $\gamma = 0.5$.

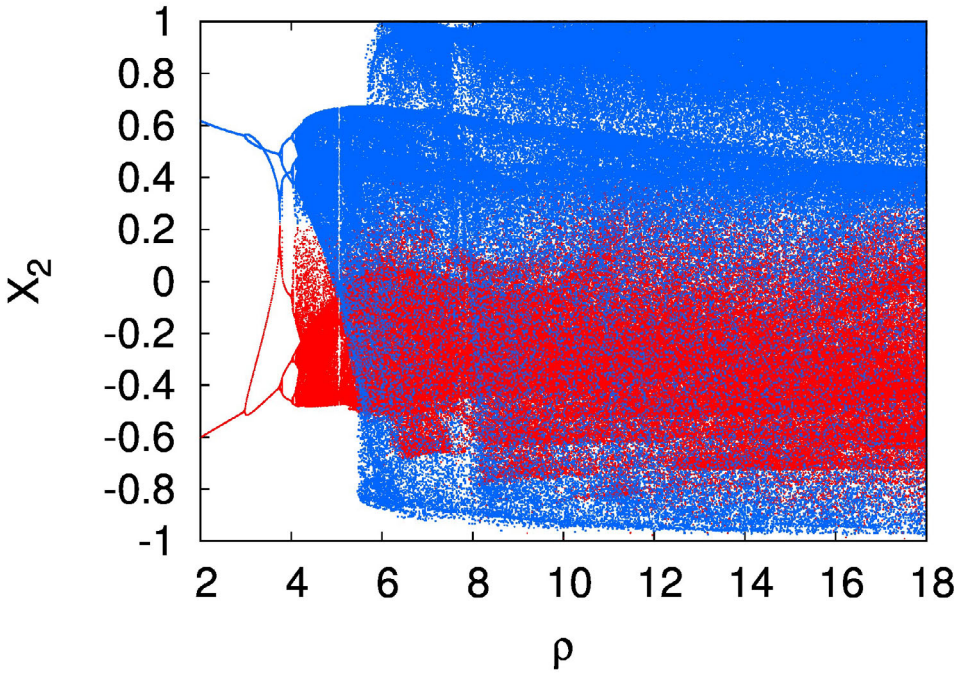


**Fig. 9.** Bifurcation diagram of the Poincaré return map of GLE-4. $X_2$ values are plotted when a trajectory of the GLE-4 system (Eq. (1)) crosses $X_1 = 0$ for $\beta = \gamma = 1$. In the color version online, points are plotted in red when $X_1' > 0$ and blue when $X_1' < 0$. Chaos appears through the period-doubling bifurcation. Figures 2 and 6 show Poincaré maps of trajectories with parameters shown in this diagram.

systems developed by Edward Lorenz, which we call generalized Lorenz equations. We have restricted study to a particular subclass of these systems for which the trajectories stay on fixed norm spheres. We further restrict to dimension 4, and norm 1, meaning that we are considering a map on the three-sphere, and have shown the rich variety of dynamics to be seen on such a system. In particular, we have seen quasiperiodicity, and Standard-Map-like coexistence of chaos and quasiperiodicity, neither of which have been seen for Lorenz systems in the past. Our explorations of this mapping on $S^3$ have been somewhat narrowly focused, leaving plenty to be done through more systematic study.

YS was partially supported by JSPS KAKENHI grant 26610034 and JST, PRESTO JPMJPR16E5. ES was partially supported by NSF grant DMS-1407087. JY was partially supported by National Research Initiative Competitive grants 2009-35205-05209 and 2008-04049 from the USDA.

## References

1. E.N. Lorenz, Deterministic Nonperiodic Flow, J. Atmos. Sci. **20**, 130 (1963)
2. E.N. Lorenz, The predictability of a flow which possesses many scales of motion, Tellus **21**, 289 (1969)
3. E.N. Lorenz, Atmospheric predictability as revealed by naturally occurring analogues, J. Atmos. Sci. **26**, 636 (1969)

4. E.N. Lorenz, Irregularity: a fundamental property of the atmosphere, Tellus **36A**, 98 (1984)
5. E.N. Lorenz, *The Essence of Chaos* (University of Washington Press, 1993)
6. E.N. Lorenz, Predictability: A problem partly solved, in *Proc. Seminar on Predictability, Vol. 1, ECMWF* (Reading, Berkshire, UK, 1996)
7. E.N. Lorenz, K. Emanuel, Optimal sites for supplementary weather observations: Simulation with a small model, J. Atmos. Sci. **55**, 399 (1998)
8. E.J. Doedel, B. Krauskopf, H.M. Osinga, Global organization of phase space in the transition to chaos in the Lorenz system, Nonlinearity **28**, 113 (2015)
9. J.L. Creaser, B. Krauskopf, H.M. Osinga, $\alpha$-flips and T-points in the Lorenz system, Nonlinearity **28**, 39 (2015)
10. R. Barrio, A. Shilnikov, L. Shilnikov, Kneadings, Symbolic Dynamics and Painting Lorenz Chaos, Int. J. Bifurc. Chaos **22**, 1230016 (2012)
11. A.E. Motter, D.K. Campbell, Chaos at fifty, Phys. Today **66**, 27 (2013)
12. C.M. Danforth, J.A. Yorke, Making forecasts for chaotic physical processes, Phys. Rev. Lett. **96**, 144102 (2006)
13. R. Capeáns, J. Sabuco, M.A.F. Sanjuán, J.A. Yorke, Partially controlling transient chaos in the Lorenz equations, Phil. Trans. R. Soc. A **375**, 20160211 (2017)
14. J.L. Kaplan, J.A. Yorke, Nonassociative real algebras and quadratic differential equations, Nonlinear Anal. **3**, 49 (1979)
15. S.N. Chow, J. Mallet-Paret, J.A. Yorke, Finding zeroes of maps: Homotopy methods that are constructive with probability one, Math. Comp. **32**, 887 (1978)